Metrology of Time-Domain Soft X-Ray Attosecond Pulses and Reevaluation of Pulse Durations of Three Recent Experiments

Xi Zhao,[1,2,*] Su-Ju Wang,[2] Wei-Wei Yu,[3,†] Hui Wei,[2] Changli Wei,[4] Bincheng Wang,[2,5]
Jigen Chen,[6] and C. D. Lin[2]

[1]*School of Physics and Information Technology, Shaanxi Normal University, Xian, Shaanxi 66506,
People's Republic of China*

[2]*Department of Physics, Kansas State University, Manhattan, Kansas 66506, USA*

[3]*School of Physics and Electronic Technology, Liaoning Normal University, Dalian 116029,
People's Republic of China*

[4]*School of Physics and Electronics, Qiannan Normal College for Nationalities, Duyun, Guizhou 558000, China*

[5]*School of Physics and Wuhan National Laboratory for Optoelectronics, Huazhong University of Science and
Technology, Wuhan 430074, China*

[6]*Zhejiang Provincial Key Laboratory for Cutting Tools, Taizhou University, Taizhou 31800, China*

Attosecond pulses in the soft x-ray (SXR) to water-window energy region offer the tools for creating and studying target-specific localized inner-shell electrons or holes in materials, enabling monitoring or controlling charge and energy flows in a dynamic system on attosecond timescales. Recently, a number of laboratories have reported generation of continuum harmonics in the hundred-electron-volt to kilovolt region with few-cycle long-wavelength mid-infrared lasers. These harmonics have the bandwidth to support pulses with durations of a few to a few-ten attoseconds. But harmonics generated in a gas medium have attochirps that cannot be fully compensated by materials over a broad spectral range; thus, realistically what are the typical shortest attosecond pulses that one can generate? To answer this question, it is essential that the temporal attosecond pulses be accurately characterized. By reanalyzing the soft x-ray attosecond metrology reported in three recent experiments [Li *et al*. 53-attosecond x-ray pulses reach the carbon K-edge, Nat. Commun. **8**, 186 (2017); Gaumnitz *et al*. Streaking of 43-attosecond soft x-ray pulses generated by a passively CEP-stable mid-infrared driver, Opt. Exp. **25**, 27506 (2017); Cousin *et al*. Attosecond Streaking in the Water Window: A New Regime of Attosecond Pulse Characterization, Phys. Rev. X **7**, 041030 (2017)] using a newly developed broadband phase retrieval algorithm, we demonstrate that the generated attosecond pulses in the first two papers have durations of about 60 as, longer than what they have reported. Similarly, the duration from the third experiment is retrieved to be about half of the 322-as upper limit cited in that work. We also introduce the autocorrelation (AC) of the streaking spectrogram. By comparing the ACs from the experiments and from the retrieved SXR pulses, the accuracy of the retrieved results can be directly visualized. Our retrieval method is fast and accurate, and it shall provide a powerful tool for the metrology of the emerging few-ten-attosecond pulses.

I. INTRODUCTION

Since the first report of isolated attosecond pulses (IAPs) in 2001 [1], the majority of IAPs are generated only in the EUV (or XUV) region, with photon energy below about 120 eV [2–4]. To study temporal electron dynamics, bond breaking, and energy flow in a biochemical reaction, extension of IAPs to the soft x-ray region (SXR) is highly desirable since SXR would excite inner-shell electrons to create a localized initial hole, which would fingerprint the flow of charges (electrons or holes) and energy, giving access to chemical processes at the most fundamental level with best spatial and temporal resolutions.

Within the last decade, the development of high-energy long-wavelength driving lasers together with pulse compression to few cycles has allowed experimentalists to generate broadband continuum high-energy photons up to 1.6 keV [5–16]. These pulses have spectral bandwidth to support transform-limited pulses of a few attoseconds or

———————
*zhaoxi719@ksu.edu
†weiweiyu@phys.ksu.edu

even zeptoseconds. However, to claim such short durations would require an accurate characterization of the spectral phase over the whole spectral bandwidth.

Recently, using two-cycle 1.80–1.85 μm lasers, three groups have reported broadband SXR harmonics [17–19]. In all three experiments, streaking spectra were also measured. Two groups reported pulse durations of 53 ± 6 as [17] and 43 ± 1 as [18], with spectral bandwidth of 100–300 eV and 65–150 eV, respectively. Both are claimed to be the shortest attosecond pulses in the world at the time. In another experiment, an upper limit of 322 as (bandwidth 150–350 eV) was reported [19]. These pulse durations were all obtained from the spectral phases retrieved from the streaking spectra. Do we have an accurate algorithm to retrieve the phase for such broadband pulses? Is there a way to check whether the retrieved phase is indeed correct? The answers to both questions, unfortunately, are not positive. Such uncertainty can easily lead to substantial error in the characterization of SXR attosecond pulses.

In this contribution, with an alternative theoretical approach and algorithm, we demonstrate that our method can accurately retrieve the spectral phase of a broadband pulse, and more importantly, we can check whether the phases have been accurately retrieved. We then use our method to re-evaluate the SXR attosecond pulses reported in Refs. [17–19], to compare their results with the ones we retrieve.

II. PHASE RETRIEVAL METHOD FOR BROADBAND ATTOSECOND PULSES

A SXR pulse in the time domain is easily obtained via Fourier transform if the electric field in the energy domain $E_{\text{SXR}}(\Omega) = U(\Omega)e^{i\Phi(\Omega)}$ is available. The spectral amplitude $U(\Omega)$, where Ω is the photon energy, can be obtained from photoelectron spectra of some rare-gas atoms ionized by the SXR alone since accurate photoionization cross sections of rare-gas atoms are available from experiments or theoretical calculations. To get information on the spectral phase $\Phi(\Omega)$, photoelectron spectra are generated by the same SXR in the presence of a time-delayed driving laser that is used to generate harmonics. The resulting electron spectra versus the time delay is called the spectrogram (or the streaking trace). The spectrogram is then analyzed to retrieve the spectral phase. In this method, it is assumed that the spectrogram can be calculated using the so-called strong-field approximation (SFA) [20,21]:

$$S(E, \tau) = \left| \int_{-\infty}^{\infty} E_{\text{SXR}}(t - \tau)d[p + A(t)] \right.$$
$$\left. \times \ e^{-i\phi(p,t)}e^{i\left(\frac{p^2}{2}+I_P\right)t}dt \right|^2, \quad (1)$$

where $E = p^2/2$ is the photoelectron energy, τ is the time delay between the two pulses, $A(t)$ is the vector potential of the laser, d is the dipole transition matrix element, I_p is the ionization potential of the atom, and $\phi(p,t) = \int_t^{\infty}[pA(t') + A^2(t')/2]dt'$ is the action of the electron in the laser field. Atomic units are used throughout the paper unless otherwise stated. The vector potential A in this equation should not be too large such that the laser cannot contribute to the ionization of the target atom.

In this model, the electron is removed by the SXR and then streaked by the vector potential of the laser until the pulse is over. To obtain the phase of E_{SXR}, previously the so-called frequency-resolved optical gating for complete reconstruction of attosecond bursts (FROGCRAB) [20,21] was used. It is based on the FROG method for retrieving the spectral phase of a femtosecond laser. To use the algorithm written for FROG, an additional approximation, called central momentum approximation (CMA), has to be made by replacing the p in the action ϕ above by the momentum of the electron at the center of $U(\Omega)$. This approximation is not severe if the bandwidth is narrow, say about 10–20 eV. Thus, earlier attosecond pulses were retrieved using the FROGCRAB method [20–22]. It is generally believed that the method works for these narrowband pulses.

To retrieve broadband pulses, the CMA has to be removed. Three methods have been proposed, phase retrieval by omega oscillation filtering (PROOF) [23], the Volkoff transform generalized projections algorithm (VTGPA) [24], and phase retrieval of broadband pulses (PROBP) [25]. PROOF is based on approximating the action ϕ in Eq. (1) by taking the limit when A is small, and that the streaking IR field is a monochromatic wave. In PROOF, the streaking shift should be small, and thus it is more sensitive to errors in the streaking spectra. PROOF was used in Refs. [17] and [22] even when the IR is a short few-cycle pulse. In the experiment of Ref. [18], the spectral phase was retrieved using the multi-line (ML) VTGPA method, which is a modification of VTGPA [24] to account for photoelectrons generated from multiple shells of the atom. In Ref. [19], the bandwidth of the SXR is about 200 eV. Using FROGCRAB, the pulse duration obtained was about 24 as. Based on the attosecond lighthouse model, it was estimated that the pulse duration should be less than 322 as.

Among the phase retrieval algorithms, including FROGCRAB, all are based on iterative methods. The calculation is terminated after tens of thousands of iterations when the merit is not changing. To "prove" that the retrieved SXR pulse (also for XUV pulse) is correct, the retrieved pulse is then used in Eq. (1) to calculate the spectrogram. By comparing the experimental spectrogram with the one from the retrieved pulse visually and ensuring that the merit has reached a specified value, it is often deemed
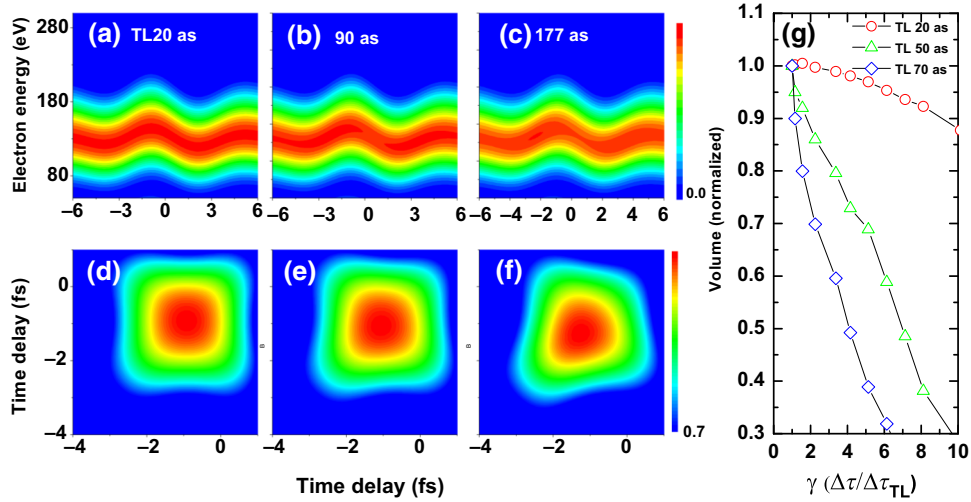
FIG. 1. Theoretically calculated spectrograms (a)–(c) and the corresponding AC patterns (d)–(f). The central energy of the three XUV pulses is 160 eV, with a FWHM bandwidth of 94 eV. The duration of the TL pulse is 20 as, while the other two are 90 and 177 as, respectively. The MIR used in the simulation is 1800 nm in wavelength, 5.7 fs in FWHM duration, and 2.5×10^{12} W/cm^2 in peak intensity. (g) Normalized volume of the AC pattern versus pulse duration in units of the duration of the transform-limited pulse. The normalized volume drops more slowly versus the scaled duration for broadband pulses than for narrowband pulses, making it harder to retrieve broadband pulses. The examples assume that the XUV pules have quadratic phases only; see text.

that the agreement is good. This procedure is probably acceptable for narrowband pulses, but not for broadband pulses.

To illustrate this point, we first compare how the spectrogram calculated using Eq. (1) depends on the spectral phase. For simplicity, consider a SXR pulse in the energy domain, $E_{\text{SXR}}(\Omega) = U(\Omega)e^{i\Phi(\Omega)}$, with a Gaussian spectral amplitude $U(\Omega) = U_0 e^{-2\ln 2[(\Omega - \Omega_0)^2/(\Delta\Omega)^2]}$ and a quadratic spectral phase $\Phi(\Omega) = a_2[(\Omega - \Omega_0)^2/(\Delta\Omega/2)^2]$. Here we use $\Omega_0 = 164$ eV as the central photon energy and $\Delta\Omega = 94$ eV as the FWHM bandwidth, which can support a transform-limited (TL) pulse (corresponding to $a_2 = 0$) of 20 as. The coefficient a_2 is a measure of the attochirp, or equivalently we can use the parameter $R = \Delta\tau/\Delta\tau_{\text{TL}}$, which is the ratio of the duration of the chirped pulse to the TL duration. Figures 1(a)–1(c) compare the spectrograms simulated according to Eq. (1). The mid-IR (MIR) used is 1800 nm in wavelength, 5.7 fs in duration, and 2.5×10^{12} W/cm^2 in peak intensity. From Figs. 1(a)–1(c), visually the three spectrograms show little difference, even though their pulse durations are 20, 90, and 177 as, respectively. To magnify their contrast, we calculate the autocorrelation (AC or Q) of the spectrogram, defined by

$$Q(\tau_1, \tau_2) = \int_0^{\infty} S(E, \tau_1)S(E, \tau_2)dE. \quad (2)$$

Figures 1(d)–1(f) show the corresponding AC patterns over one optical period. For the TL pulse, the AC shape is close to a square in the center. As the linear chirp is

increased, the square gradually deforms and skews along the diagonal axis. Clearly, the greater the deformation, the larger the linear chirp (and pulse duration). To delineate the relative deformation of the AC with respect to the TL pulse, we define a normalized volume V_{norm} for each AC pattern:

$$V_{\text{norm}} = \frac{\iint Q(\tau_1, \tau_2)d\tau_1 d\tau_2}{\iint Q^{TL}(\tau_1, \tau_2)d\tau_1 d\tau_2}, \quad (3)$$

in which we integrate the AC pattern (transform-limited AC pattern) over an area of half an optical cycle T along each axis centered at the coordinate with the maximum value of the AC pattern (transformed-limited AC pattern). Figure 1(g) shows that V_{norm} drops very quickly with R if the TL pulse is 70 as, but very slowly if the TL pulse is 20 as. This tells us that attosecond pulses with a broader bandwidth are much more difficult to retrieve. The MIR used for Fig. 1(g) has a wavelength of 1800 nm.

PROBP was first introduced in Ref. [25], where the unknown laser and/or SXR are to be retrieved from the spectrogram. It does not impose the central momentum approximation. In PROBP, the spectral amplitude $U(\Omega)$ of the SXR is known from the experiment. The unknown vector potential of the streaking MIR field is also expressed in the energy domain

$$A(\Omega) = f(\Omega)e^{i\Psi(\Omega)}. \quad (4)$$

Each of the unknown functions $\Phi(\Omega)$, $f(\Omega)$, and $\Psi(\Omega)$, respectively, is expanded in terms of B-spline basis

functions

$$f(x) = \sum_{i=1}^{n} g_i B_i^k(x). \tag{5}$$

With some guessed parameters of these unknown functions, the constructed SXR and MIR are used in Eq. (1) to obtain the spectrogram. By comparing the resulting spectrogram with the experiment, a genetic algorithm is used to select the new guesses for the next iteration. The iterative process is terminated after tens of thousands of steps or after some preselected merit is reached. The PROBP method has been shown to work well for pulses with bandwidth up to about 100 eV [25]. The convergence becomes much slower for pulses with larger chirps or broader bandwidths.

Since the AC appears to be a more sensitive marker of the spectral phase than the spectrogram, in the PROBP AC method [26], we retrieve the phase directly from the experimental AC patterns. The fitness function is defined as the sum of

$$E_f = \sum_{i,j} \min\left[Q_0(i,j), Q_1(i,j)\right], \tag{6}$$

where Q_0 and Q_1 are the normalized input AC from the experiment and the reconstructed AC, respectively. The $\min(x, y)$ is defined as the smaller of x and y. If the input and the reconstructed ACs are exactly the same, the fitness function is equal to 1. In the numerical computation, we discretize the spectrogram $S(E, \tau)$ and the AC pattern $Q(\tau_1, \tau_2)$ on grid points. We use the genetic algorithm (GA) to find the optimal parameters that would minimize the function $(1 - E_f)$ defined in Eq. (6).

For narrower bandwidth pulses, previous studies [26] show that the PROBP AC method converges much faster and more accurately in examples where the FROGCRAB, the PROBP, and the PROBP AC method could all retrieve successfully. For the broadband pulses discussed here, we use the PROBP AC method only since the PROBP method does not converge or take a long time to reach convergence. Besides the sole application of the PROBP AC method to the three experiments in this work, we point out that the fitness function in Eq. (6) is used here to replace the familiar rms method as used in Ref. [26], whose fitting strategy is to use all the data points on an equal footing including those with large errors. The method used in Eq. (6) requires that at each iteration the fitted AC be a smooth function and that the sum of $Q(i,j)$ over the block be normalized, for the experimental data and for the theoretical ones calculated at each iteration. By taking the smaller of AC at each (i,j) point in Eq. (6), the sum (fitness) will become less than one. The iteration is to make this sum get as close to one as possible, which would fit the experimental data exactly. This method has the effect of downplaying the importance of spikes in the data points and is in favor of achieving a globally smooth distribution of the fitted data. We also find that this approach converges faster since it reaches convergence monotonically.

Last but not the least, we comment on the philosophy of introducing the PROBP AC method for improving the phase retrieval of broadband pulses. Since a mid-infrared driving laser is utilized for streaking, at each time delay, the photoelectron spectrum covers a wide range of energies. In addition, if a long optical period of the mid-infrared laser is used, more points in time delay are needed. Generating such a large amount of data points in streaking spectra is difficult in experiments by itself; at the same time, it poses a challenge for retrieving the spectral phase. By introducing the autocorrelation in Eq. (2) from the streaking spectra and limiting the time delay interval to only one optical cycle, it reduces the number of data points to be used for the analysis. Notice that the usage of AC is not the only way to achieve this goal. For example, one can introduce different kinds of moments [distinct from Eq. (2)] that would serve the same purpose. By analyzing the AC, the noise in the streaking spectra to some extent also is averaged out. The smaller data set alone also makes the PROBP AC method computationally much faster.

III. NEW RETRIEVAL OF ATTOSECOND PULSES FROM PREVIOUS EXPERIMENTAL DATA

To elaborate the advantage of using the AC instead of the spectrogram for spectral phase retrieval, in Figs. 2(a) and 2(e), we show the spectrograms from experiment with the one obtained from the retrieved pulse reported in Ref. [18]. We calculate the ACs from these two spectrograms, and the results are shown in Figs. 2(b) and 2(f). The AC patterns are expected to repeat reasonably well for each optical cycle of the MIR laser. We label several blocks (blocks 1–7), and one can see that the ACs from the experiment and from the simulated pulse do not agree well. Similarly, in Figs. 2(c) and 2(g), the spectrograms from the experiment and from the simulated pulse of Ref. [17] are compared, and their corresponding ACs are compared in Figs. 2(d) and 2(h). Clearly, the latter shows that the experimental one and the retrieved one do not match well. Such a discrepancy means that the SXR pulses reported in these experiments were not accurately retrieved. These results also demonstrate that the ACs serve as a good metric for evaluating the quality of the broadband SXR pulses retrieved, independent of whatever retrieval method is used.

Here, first we report the reanalysis of the data from Ref. [18]. In this experiment, the pulse was retrieved from the ML VTGPA method. Here we use the PROBP AC method. The experimental streaking spectra shown in Fig. 2(a) covers a few optical cycles but they do not repeat very well as expected. In particular, in the region near
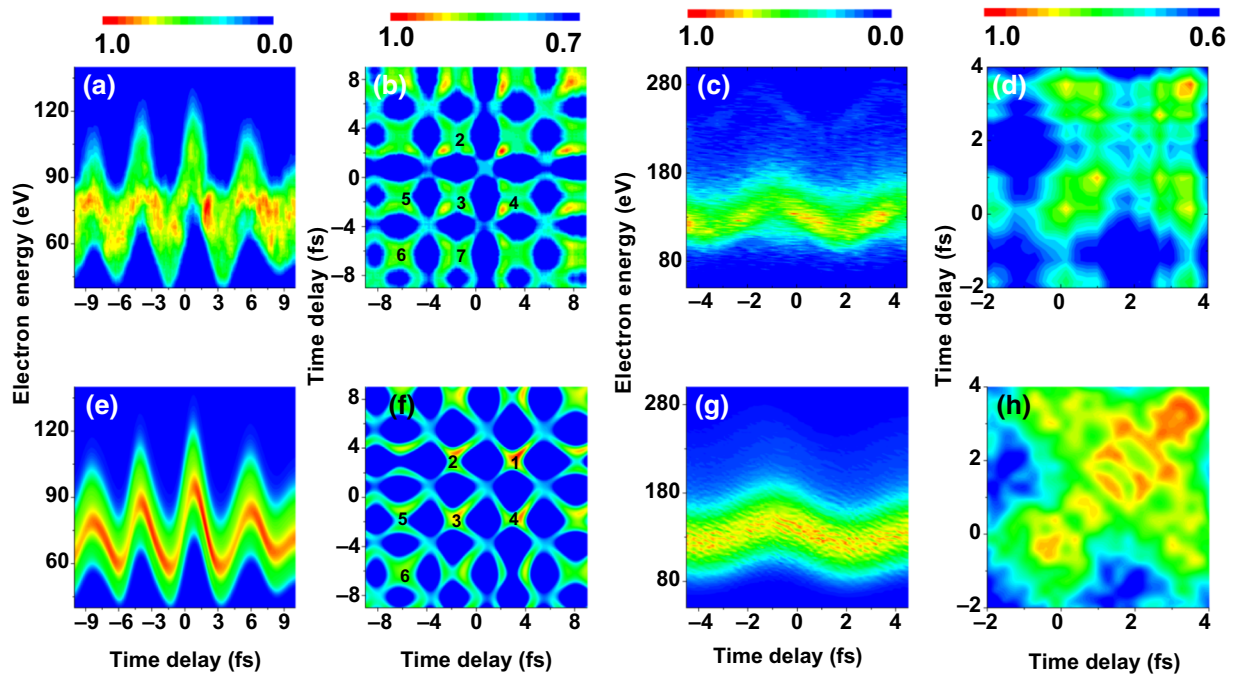
FIG. 2. Experimental spectrograms and corresponding AC patterns. The two left columns are from Ref. [18] and the two right columns are from Ref. [17]. The upper row data are from the experiments and the lower row data are from the reconstructed theoretical data using the retrieved SXR and MIR pulses. Each pair along the column should match well if the retrieval is accurate.

$(E, \tau) = (75 \text{ eV}, 2 \text{ fs})$, the spectrogram signal is about 30%–40% higher. From Fig. 2(a), it appears that the data from $\tau = -9$ fs to -1 fs is better behaved, thus we choose to analyze the AC in block number 5 as the best case. Analysis has also been made for other blocks. They are documented in the second paragraph of Appendix B.

The ACs for block number 5 from the experimental and the retrieved pulses from Ref. [18] are shown in Figs. 3(a) and 3(b), respectively. We can see that they show little resemblance. Using our PROBP AC method, the resulting AC is shown in Fig. 3(c). It is much closer to the experimental data given in Fig. 3(a). In our PROBP AC method, the spectral amplitude of the SXR is obtained from the experiment. The vector potential of the 1800-nm MIR laser is also retrieved. From our results, we reconstruct the intensity of the SXR in the time domain, see Fig. 3(d). Our result does not agree very well with the one reported in Ref. [18]. The FWHM pulse duration from our new evaluation is 62 as, as compared to 43 as reported in Ref. [18]. In Fig. 3(e), we compare the spectral phases. The phase obtained in Ref. [18] is very small over the whole spectral range, and thus they retrieved a near-TL pulse. Our result from PROBP AC shows large chirps away from the central energy. Note that the linear term in the spectral phase has been removed. Thus, the spectral phases presented in Fig. 3(e) show the phases that contribute to the pulse duration beyond the TL pulse. The reason for the discrepancy between the present result from Ref. [18] is further discussed in Appendices B

and C. On the other hand, the better agreement of Fig. 3(c) than Fig. 3(b) with the experimental data Fig. 3(a) is a good indication that the present retrieved result is more accurate. We can also calculate the merit of the retrieved pulses (see Appendix D) using the AC or the spectrogram. From the AC, our (Ref. [18]) merit is 0.03 (0.09), and from the spectrogram is 0.010 (0.019), both showing our method obtains better merits. Figure 3(f) compares the retrieved vector potential of the two methods. On femtosecond timescales the agreement between the two retrieved vector potentials is quite good.

Next we re-examine the SXR pulse generated by a two-cycle pulse near 1.8 μm reported in Ref. [17]. Their spectrum extends from about 100 to 300 eV; the bandwidth is 94 eV and the TL pulse is 20 as. This pulse was retrieved in Ref. [17] based on the PROOF method, which approximates the SFA, Eq. (1), under the condition that the streaking MIR is monochromatic and that the vector potential of the MIR is very weak. In this experiment, the target atom for the streaking spectra is helium. Figure 4 summarizes the retrieved results of Ref. [17] using PROOF and from our PROBP AC method. Figure 4(c) shows the AC from our retrieved result. It agrees better with the AC from the experimental data in Ref. [17] shown in Fig. 4(a) than the AC obtained from the retrieved SXR using PROOF [Fig. 4(b)]. The pulse duration retrieved from our method is 61 as, while from PROOF it is 53 ± 6 as. Even though the pulse durations are quite close, the PROOF result
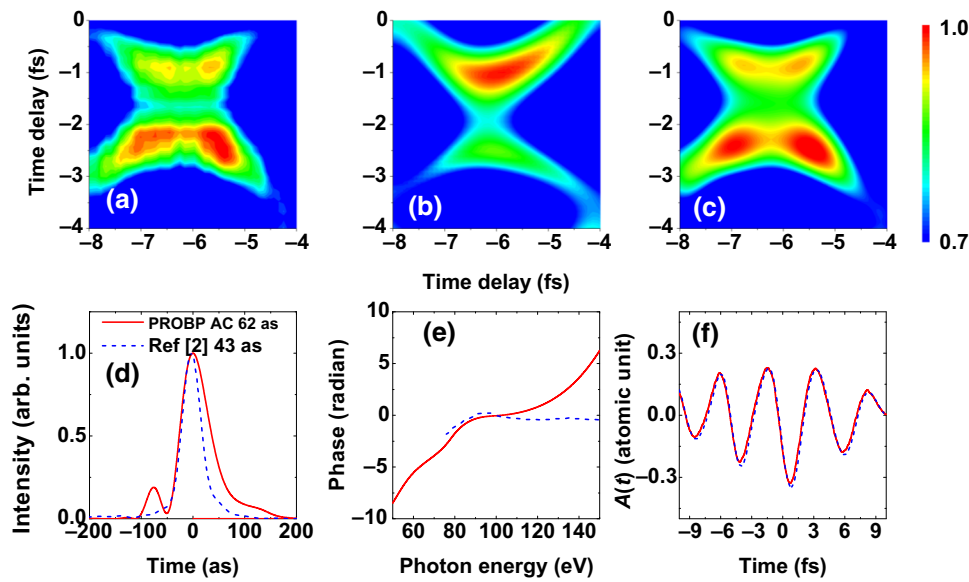
FIG. 3. (a) Experimental AC pattern and (b) the retrieved AC pattern from Ref. [18]. (c) The retrieved AC pattern from the present method. (d) The retrieved temporal intensity envelope, (e) the spectral phase of the SXR, and (f) the vector potential of the MIR. The retrieval is obtained from the AC pattern of block 5 in Fig. 2(c). In (d)–(f), the solid red lines are from the present retrieval method and the blue dashed lines are from Ref. [18].

shows a larger spectral phase change from 50 eV to 300 eV. Such large phase variation results in a structured long tail of the SXR pulse in the time domain, as seen in the blue-dashed line of Fig. 4(d). Note that the intensity of the second peak there is about 0.34 of the central peak, and thus the electric field at the second peak is 60% of the main peak. The result from PROBP AC gives a smaller spectral phase, and a much better behaved SXR pulse in the time

domain, see the red line in Fig. 4(d). The retrieved two-cycle MIR pulse is shown in Fig. 4(f) (the PROOF method assumes that the MIR is monochromatic). Based on the comparison of the ACs in Fig. 4, it is fair to say that the PROBP AC result is more accurate. This is also supported by the merits between this work and the PROOF method, 0.036 vs 0.061 based on the ACs, or 0.012 vs 0.032 using the spectrograms (see Appendix D).
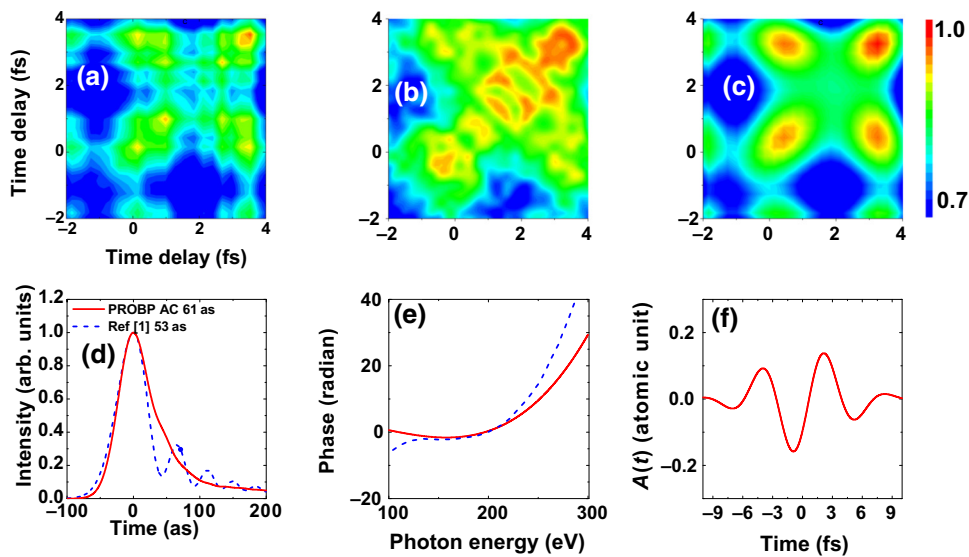
FIG. 4. (a),(b) AC patterns from the experimental and the retrieved spectrograms reported in Ref. [17], respectively. (c) Reconstructed AC pattern from the present method. (d) Temporal intensity envelopes of the SXR. (e) Spectral phase of the SXR retrieved and (f) vector potential of the MIR retrieved from the present method. In (d) and (e), the red solid lines are from the present method, and the blue-dashed lines are from the PROOF results of Ref. [17].
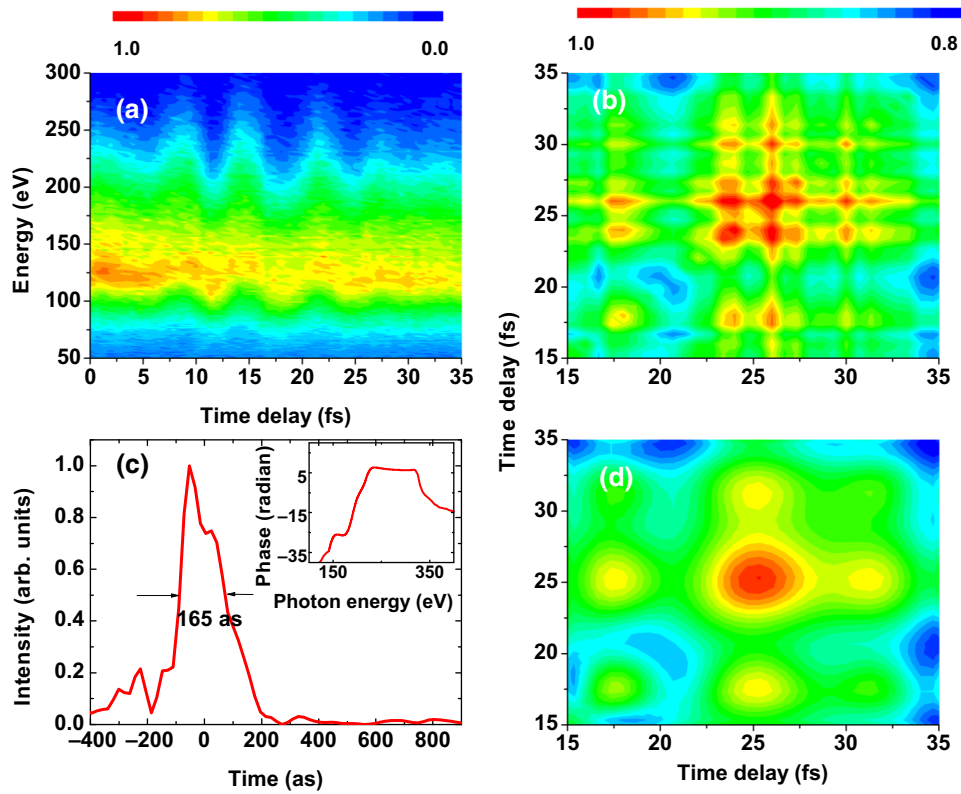
FIG. 5.   (a),(b) Experimental trace and the derived AC pattern from Ref. [19], respectively. (d) The AC obtained from the present retrieved pulse. It is only in marginal agreement with the one in (b). (c) Envelope of the temporal intensity of the SXR; the inset is the spectral phase. Both are from the present retrieval method.

We also retrieve the streaking data from Ref. [19]. The central photon energy of the SXR is at 250 eV, with a bandwidth of about 200 eV, corresponding to a TL pulse of about 10 as. Ionization of the SXR on Kr atoms would generate most of the photoelectrons from the 3*d*. Figure 5(a) shows the experimental spectrogram. Due to the weak signal, the spectrogram does not show clean oscillation with respect to the optical period of the mid-IR pulse. Since the spectrogram shows good oscillatory behavior from 15 to 35 fs in Fig. 5(a), we calculate the AC in this range, and the result is shown in Fig. 5(b). Using this AC pattern, we retrieve the spectral phase. The retrieved time-domain intensity profile is shown in Fig. 5(c). It has a FWHM pulse duration of 165 as, about half of the upper limit of 322 as reported in Ref. [19] based on the attosecond lighthouse model. The spectral phase obtained from our retrieval method is given in the inset of Fig. 5(c). Comparing the AC using the retrieved pulses, as shown in Fig. 5(d), it does show an overall global agreement with Fig. 5(b), but clearly the details are different. Due to the broader bandwidth and higher photon energies and thus the weaker signals and longer time (about 10 h) in collecting the spectrogram, it is not clear that the 165-as duration retrieved is the "shortest" pulse that can be obtained for this broadband pulse. Since broader bandwidth would incur

larger chirps in the spectral phase away from the center, a shorter TL pulse may not necessarily be a better way for generating a shorter attosecond pulse below 50 or 60 as.

Before concluding this section, we mention that additional details about our retrieval methods are given in the appendix. In Appendix B we present pulses retrieved from different blocks. In Appendix D we compare the streaking spectra from the experiment with the one we retrieved. We also report the pulse retrieved from all the blocks covering the full time delay period carried out in the experiment, instead of just one block. Finally we confirm that the pulse derived from the PROBP AC cannot be further improved by using PROBP, with the initial input from the result of PROBP AC, to retrieve the pulse from the streaking trace.

IV. DISCUSSION

One of the grand challenges of ultrafast and attosecond physics is to generate even shorter light pulses in the soft x-ray region for probing inner-shell electron dynamics of materials. Often it was assumed that one would just have to keep generating continuum harmonics over ever increasing bandwidth. This would work if the spectral phase can be compensated over the whole broad energy region. As addressed in Ref. [19], there is still no practical method

available to do that. In the meanwhile, accurate phase retrieval of a broadband pulse using the spectrogram has been shown to be very slowly converging. In this work, we show that phase retrieved directly from the autocorrelation of the spectrogram is more efficient and more accurate. We also demonstrate that correct phase is retrieved when the AC from the experimental data agrees with the AC from the retrieved pulse. The PROBP AC method is expected to provide a faster and more accurate tool for characterizing narrow as well as broadband attosecond pulses in the future, to enable temporally well-characterized attosecond SXR pulses for studying ultrafast electron dynamics in matter.

APPENDIX A: SENSITIVITY OF THE AC PATTERN TO ATTOCHIRP ON THE WAVELENGTH AND INTENSITY OF THE IR LASER FIELD

The sensitivity of the AC pattern to attochirp (only linear chirp is considered in this section) on the wavelength and intensity of the IR laser field is illustrated in Figs. 6(a) and 6(b). We define a parameter R, which is the ratio of the duration of the chirped pulse to the duration of the transform-limited pulse (20 as in this case), to indicate the amount of attochirp. The change of the metric volume from the autocorrelation pattern as a function of R, i.e., the slope in Fig. 6, reflects how easily the SXR or XUV pulses can be retrieved. A larger slope means a better sensitivity to the spectral phase, which leads to a faster convergence and a better performance of the phase-retrieval process. Ideally one would like to choose intensity and wavelength of the streaking laser field that give steeper slopes in Figs. 6(a) and 6(b) if possible.

The laser parameters used in Fig. 6 are the same as those in Fig. 1 except for the IR intensities and wavelengths. In Fig. 6(a), we fix the IR intensity to 2.5×10^{12} W/cm^2 and vary its wavelength. The metric volume decreases monotonically with R in all cases. Based on our calculations for three different wavelengths, the best sensitivity is achieved at 800 nm, while the performance becomes lower when we
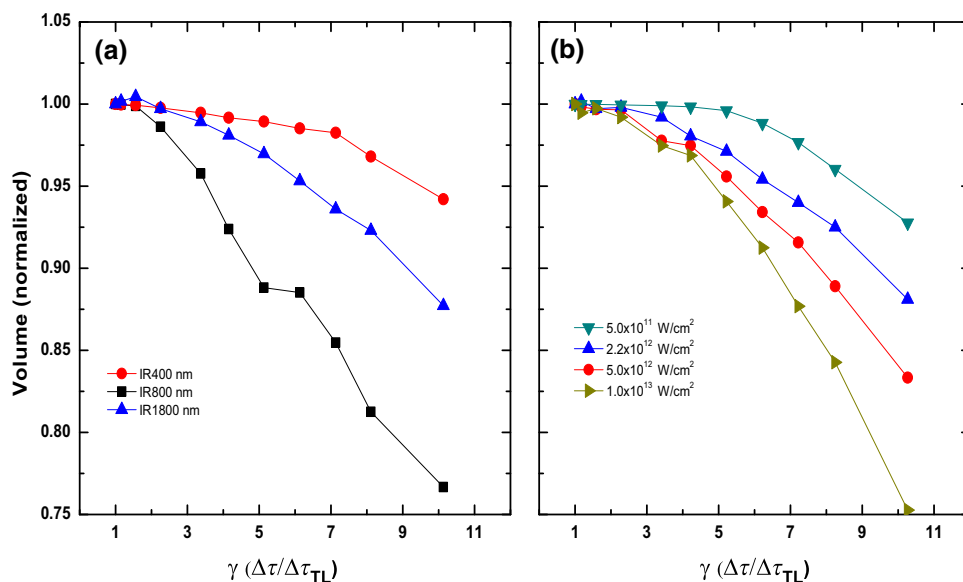
FIG. 6. The normalized volume of the autocorrelation pattern as a function of R, which is the pulse duration ratio between the linearly chirped pulse and the TL one. In (a), the IR intensity is fixed at 2.5×10^{12} W/cm^2 and the IR wavelengths are chosen to be 400, 800, and 1800 nm. In (b), the IR wavelength is fixed at 1800 nm and four intensities are used.

either increase the wavelength to 1800 nm or decrease the wavelength to 400 nm.

In Fig. 6(b), we plot the dependence of the metric volume from the AC pattern as a function of R for various IR intensities at the fixed IR wavelength 1800 nm. It is shown that the slope decreases with decreasing IR intensity, which indicates that the streaking contrast is weaker at a lower IR intensity and makes the retrieval method less sensitive to the spectral phase. This would imply that the low IR intensity required for the PROOF method is less favorable.

APPENDIX B: EFFECT OF MULTIPLE PHOTOIONIZATION CHANNELS

In Fig. 3, our PROBP AC method accounts for photoelectrons ejected from the $5p$, $5s$, and $4d$ subshells of Xe. It is noted that in Gauminitz *et al.* [18], only $5p$ and $5s$ electrons are included. Figure 7 shows the yields of photoelectrons, which is given by the product of dipole intensity and the XUV intensity $|d(E)|^2 |E_{XUV}(E)|^2$, for each of the three channels. The dipole data and the XUV intensity, as functions of the photoelectron energy E, are identical to those used in Ref. [18]. Note that from 40 to 60 eV, the dominant contribution to the photoelectron spectra is from the $4d$ channel. In the range from 60 to 75 eV, both $5p$ and $5s$ channels have significant contributions to the spectra. The $4d$ channel becomes insignificant for electron energy above 63 eV. Above 75 eV, the $5p$ channel becomes the dominant channel. As the energy is above 80 eV, the intensity of the $5p$ channel is at least 1 order of magnitude larger than those from the $5s$ and $4d$ channels.

Figure 8 shows the retrieved spectral phase and Fig. 8 shows the retrieved intensity of the XUV in the time
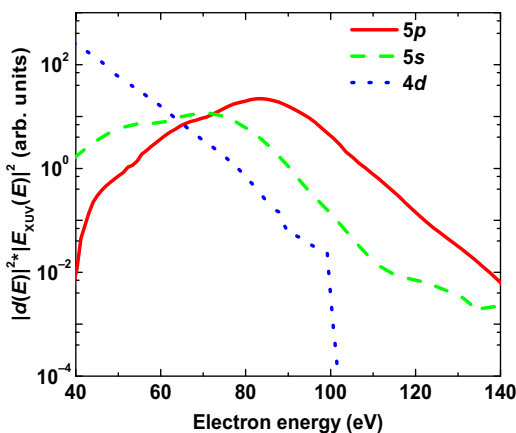
FIG. 7. Contributions of photoelectrons from different subshells to the ionization of Xe by the SXR in the experiment of Ref. [18]. The photon energy is expressed as $E + I_P$ for each subshell. The sharp cutoff near 100 eV for $4d$ shell is due to the spectral range of the SXR pulse.

domain, by including only $5p$, and only $5s$ and $5p$, respectively, and are compared to results including all three channels. By including all three channels we obtain pulse duration of 62 as. By including only one or two channels, the retrieved pulses are 74 and 72 as, respectively. For comparison, in Ref. [18], only the $5p$ and $5s$ channels were included and they retrieved a pulse duration of 43 as.

1. Dependence of phase retrieval from different blocks

The PROBP AC methods can retrieve the pulses from just one block of the AC, or from a few blocks. By covering the spectrograms over a few MIR optical cycles may in principle average over the noises in the signals. However, this procedure is preferred only if the noises are completely random. In the main text, by analyzing the spectrogram in Fig. 2(a), we noted that the spectrogram taken before $\tau = 1$ fs appears to be better behaved. Thus, we chose block 5 to retrieve the XUV and the MIR pulses, to obtain the results shown in Figs. 3(d)–3(f). Indeed, the spectrogram in Fig. 2(a) is found to have 30–40% higher signals in the region near $(E, \tau) = (75 \text{ eV}, 2 \text{ fs})$. Such singular behavior is not expected in the spectrogram and it is likely due to noises. Thus, phase retrieval including data from this region is less desirable. To elaborate this point, we note that blocks 1 and 2 (which is equivalent to 4) contain data from this undesirable region, while blocks 3, 5 (equivalent to 7), and 6 do not contain those data. We use the same retrieval method and dipole parameters as we use in analyzing block 5 to analyze blocks 1, 2, 3, and 6. The results are shown in Figs. 9 and 10. In Fig. 9, on the top row, the ACs of each block obtained from the experiment of Ref. [18] are compared to the ACs generated from our retrieved pulses, shown in the bottom row, respectively. Clearly, one can see that they exhibit very good overall agreement for each pair. In Fig. 10(a), the spectral phases retrieved from blocks 1 and 2 are very close to each other, but they are very different from the ones retrieved from blocks 3 and 6. We note that the latter are in good agreement with the one reported in Fig. 3(e) retrieved from block 5. In fact, from blocks 3, and 6, we retrieved pulse durations of 61 as and 60 as, respectively, which are very close to the 62 as retrieved from block 5. In contrast, from blocks 1 and 2, we retrieve pulse durations of 90 as, and 80 as, respectively. The intensity profile in the time domain for the five retrieved pulses is shown in Fig. 10(b). Results from blocks 1 and 2 are quite different from blocks 3, 5, and 6. Based on these results, we suggest that the "noise" in the spectrogram near $(E, \tau) = (75 \text{ eV}, 2 \text{ fs})$ in Ref. [18] contributes to this difference. We also note that pulse duration alone is not a good representation of the temporal behavior of the SXR attosecond pulses since the intensity profile can still differ significantly, see the intensity profile obtained from block 3 as compared to those from blocks 5 and 6 in Fig. 10(b).
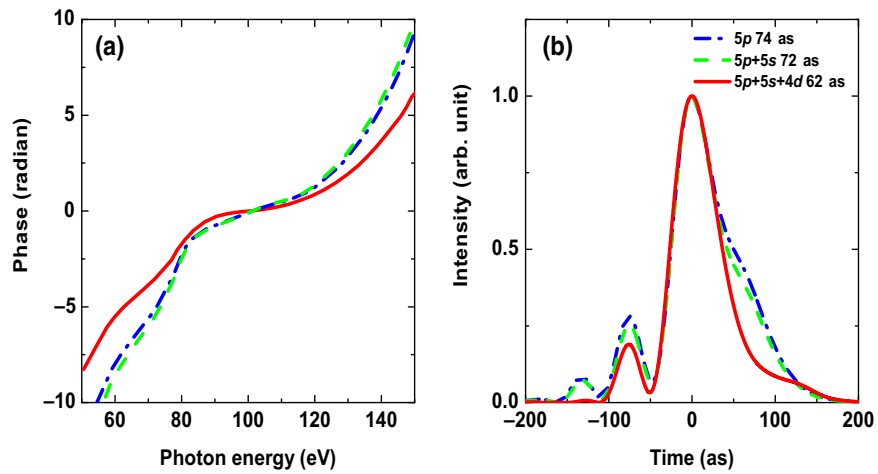
FIG. 8. (a) Retrieved spectral phases with inclusion of 5*p* channel only (red solid), 5*p* + 5*s* channels (green dashed), and all three 5*p* + 5*s* + 4*d* channels (blue dotted). (b) The corresponding retrieved temporal intensity envelopes, respectively.
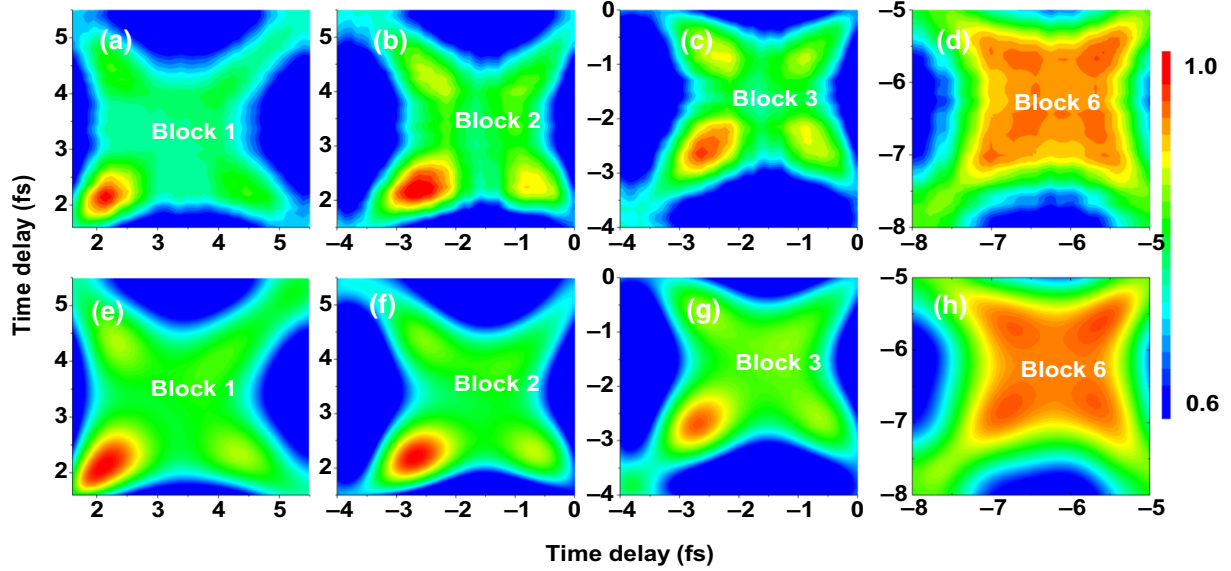
FIG. 9. Experimental AC patterns (a)–(d) and their corresponding AC patterns (e),(f) retrieved using the PROBP AC method for the four blocks indicated. Good agreement has been achieved in each case.
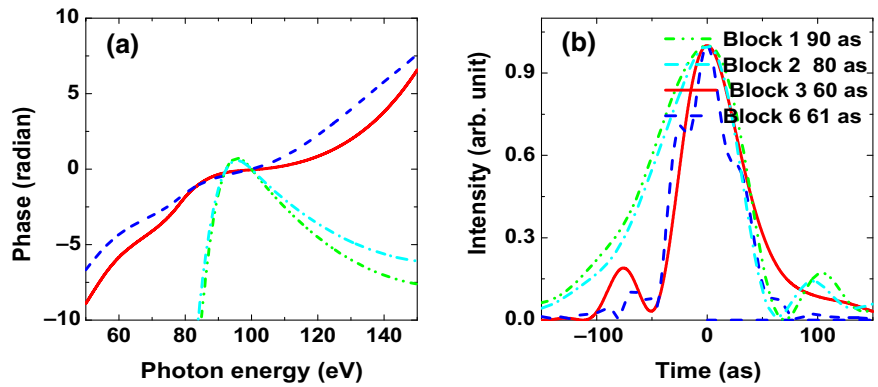
FIG. 10. Retrieved spectral phases (a) and the temporal intensity envelopes for for blocks 1, 2, 3, and 6, respectively.

TABLE I. Merits of the streaking traces (ε_S) and the AC patterns (ε_{AC}) for the experimental data of Ref. [18] obtained using different retrieval methods. The merit from ML VTGPA is obtained from the spectrogram retrieved in Ref. [18].

	ε_S	ε_{AC}
PROBP AC (with $5p + 5s$)	0.012	0.042
PROBP AC (with $5p + 5s + 4d$)	0.010	0.030
ML VTGPA (with $5p + 5s$)	0.019	0.090

TABLE II. Merits of the streaking traces (ε_S) and the AC patterns (ε_{AC}) for the experimental data of [17]. To obtain the merits for the PROOF method, we generate the spectrogram based on the published pulse parameters in the cited paper, and the MIR laser is assumed to be monochromatic as in the PROOF model.

	ε_S	ε_{AC}
PROBP AC	0.012	0.036
PROOF	0.032	0.061

APPENDIX C: COMPARISON OF MERITS

To compare the difference between the experimental and retrieval results, we define the merit by

$$\varepsilon_f = \frac{\sum_{i=1}^{M} \sum_{j=1}^{N} \left| f_{\text{output}}(i,j) - f_{\text{exp}}(i,j) \right|^2}{\sum_{i=1}^{M} \sum_{j=1}^{N} \left| f_{\text{exp}}(i,j) \right|^2}, \quad \text{(C1)}$$

where $f_{\text{output}}(i,j)$ is the two-dimensional output from the retrieval, $f_{\text{exp}}(i,j)$ is the experimental data, M and N are the number of grid points on the time delay and the photoelectron energy, respectively. The function f can be the streaking trace (S) or the AC pattern. Before making any comparison, we normalize streaking traces and AC patterns with respect to their maximum values such that they have values between 0 and 1. If the retrieval results $f_{\text{output}}(i,j)$ match perfectly with the experimental data $f_{\text{exp}}(i,j)$, then the merit $\varepsilon_f = 0$. We calculate the traces and ACs using the SXR phases and vector potential of the MIR retrieved from the PROBP AC method.

Table I summarizes the merits for the retrieval of experimental data based on our PROBP AC method and with the retrieved pulse using ML VTGPA from Ref. [18]. We use 40×40 grid points for the AC in the region of $\tau_1 \in [-4 \text{ fs}, 0 \text{ fs}]$ and $\tau_2 \in [-8 \text{ fs}, -4 \text{ fs}]$ for the retrieval and merit calculations. More points are used for comparison of the streaking traces. A total of 200 grid points in time delay axis (-10 to 10 fs) and 320 grid points in energy axis (40 to 140 eV) are used. Table I shows that the merit using the PROBP AC method including $5p$, $5s$, and $4d$ channels give the best merits, using both the streaking spectrogram or the AC pattern. If the contribution of photoelectrons from $4d$ is not included, i.e., only including $5s$ and $5p$, then the merits increase slightly, meaning that the retrieval is not as good as the one including all three channels. This is consistent with the results in Fig. 8. On the other hand, the merits calculated using the experimental and the retrieved spectrograms provided from Ref. [18] show significantly larger merits, for both calculated from the streaking traces or from the AC patterns. Based on the comparison of the AC patterns in Fig. 3 of the main text and the merits shown in Table I, we believe it is fair to claim that the SXR pulses retrieved from this work is more accurate.

Similarly, we compare the merits using the experimental data of Ref. [17]. We use 121×121 grid points for the AC

in the region of $\tau_1 \in [-2 \text{ fs}, 4 \text{ fs}]$ and $\tau_2 \in [-2 \text{ fs}, 4 \text{ fs}]$. A total number of 160 grid points in time delay axis (-4 to 4 fs) and 40 grid points in energy axis (50 to 350 eV) are used for the streaking traces. The results are shown in Table II. Note that the retrieved spectrogram used for the analysis is generated by us using the pulse parameters reported in Ref. [17]. From Table II, we note that in both cases, the PROBP AC method gives smaller values for the merit, thus demonstrating that the SXR pulses are more accurately retrieved using the PROBP AC method than reported in the original paper.
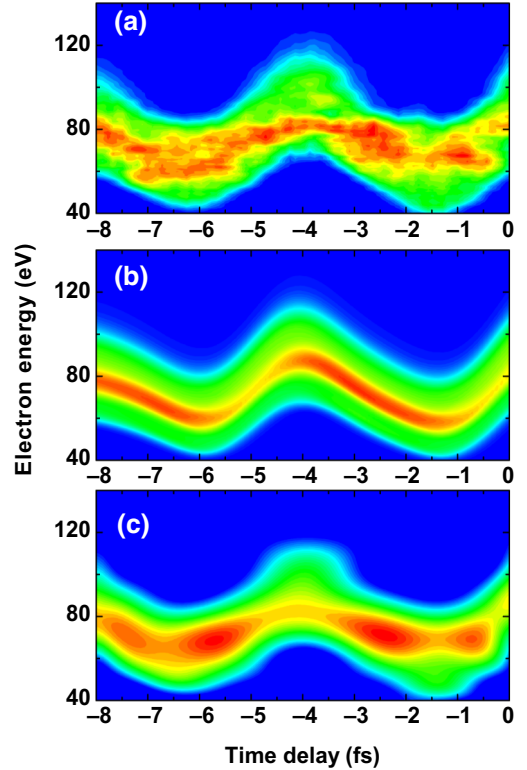
FIG. 11. Part of the streaking traces (a) from the experiment of Ref. [18], see Fig. 3. In (b) and (c), the generated streaking traces using the SXR pulses retrieved from the experimental paper and from the present PROBP AC method are shown. One is able to see that (c) is in better agreement with (a) than (b) with (a). However, the contrast in the streaking traces is not as good as the ACs shown in Figs. 3(a)–3(c) in the main text.

The efficiency of the GA depends sensitively on the choice of B-Spline functions parameters, the order k and the number of B-spline functions n. Experimenting on the choice of the input parameters for the GA is necessary. Our strategy to overcome the problem is to run over different combinations of (n, k) for a few generations (about 200 in this work) and pick the basis set with fastest descent in fitness function. Based on our observations, running k from 5 to 7 and n from 10 to 14 would often guide us to select the best n and k for our cases. One last freedom in the B-spline basis function is how one places the $(n + k)$ knots in the energy regime of interest. Our experiences show that placing more knots near the central energy of the XUV pulse always allows a faster evolution of the GA to the optimal solution. Details of the technical of GA and B-spline functions can be found in Ref. [26] of the main text.

All the calculations converge at about 2000 generations (2 h).

APPENDIX D: ADDITIONAL TESTS ON THE PROBP AC RESULTS

In the main text, we focus on the retrieval of the SXR pulses using only one block of the autocorrelation pattern.

Using block 5, in Figs. 3(a)–3(c) we demonstrate that the AC from the experimental data is much more accurately reproduced from our retrieved pulse than the one reported in Ref. [18]. One would like to see such a comparison on the streaking traces as well since it is the actually measured experimental data. Figure 11 provides such a comparison for the streaking trace from $t = -8$ to $t = 0$ fs, see Fig. 2(a) in the main text. From this figure (Fig. 11), one can definitely say that the streaking trace generated from PROBP AC (c) is in better agreement with the experiment (a) than the one retrieved in Ref. [18](b). One notes, however, the contrast of streaking traces in Fig. 11 is not as sharp as the ACs seen in Figs. 3(a)–3(c). This is in agreement with Fig. 1 in the main text. It is the main reason for us to favor the retrieval from the AC patterns.

In Figs. 9 and 10, we show that pulse durations retrieved from blocks 3 and 6 give the pulse duration of about 61 as. These blocks are generated from streaking spectra for negative time delays ($t < 0$) in Fig. 2(a) in the main text. In this figure, a strong signal is seen near $t = 3$ fs in the streaking spectra. Using blocks 1 and 2, where each block covers this strong signal, we obtain the pulse duration of 90 and 80 as, respectively. In the main text, we report pulse durations of these two portions of the streaking spectra
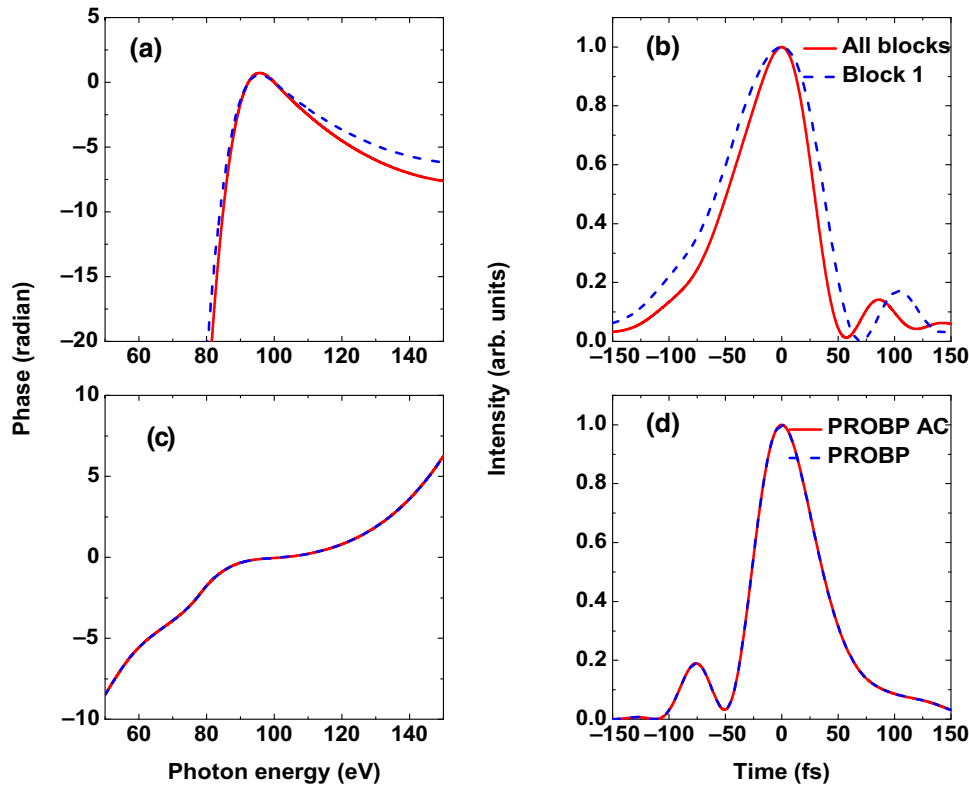
FIG. 12. Comparison of spectral phase and temporal intensity for SXR pulses retrieved from all blocks (red lines) with the pulse retrieved from block 1 alone. The retrieved pulse durations are 85 as and 90 as, respectively. See text for more explanation. (c),(d) Calculations to show that PROBP AC results are converged. By running PROBP for another 10 h on the streaking spectra using the pulse retrieved from PROBP AC as the input for another 10 h, we did not see any visible change from the input pulse, which took only 90 min.

separately since we believe that the localized strong signal in the streaking spectra is not expected. Clearly one can argue that the whole streaking spectra should be analyzed together. In Figs. 12(a) and 12(b) we report the results by analyzing all the blocks using PROBP AC. The spectral phase and the temporal intensity of the SXR obtained using all the blocks of the whole streaking trace are compared to the one obtained from block 1. It shows that the retrieved SXR is 85 as—close to the 90 as from block 1 alone. This is not surprising since the localized strong signal (30% higher) dominates the whole streaking trace.

Another issue that one might raise is whether the retrieved pulse using PROBP AC, which is based on the AC alone can be further improved. This can be done using the result from PROBP AC as the input to the PROBP method where the experimental streaking trace is directly used for the retrieval. In Figs. 12(c) and 12(d) we show that further iterations using PROBP on the streaking trace has not produced any noticeable change on spectral phase and the temporal intensity profile. In obtaining the results shown in Figs. 12(c) and 12(d), the PROBP AC method took 90 min. We then continue and run PROBP for another 10 h. No improvement is found.

This is consistent with our prior tests (not shown) based on theory-generated data that the PROBP AC method can retrieve the input phase of the SXR pulse accurately, whereas the PROBP was unable to reach convergence.

---

[1] M. Hentschel, R. Kienberger, C. Spielmann, G. A. Reider, N. Milosevic, T. Brabec, P. Corkum, U. Heinzmann, M. Drescher, and F. Krausz, Attosecond metrology, Nature (London) **414**, 509 (2001).

[2] C. D. Lin, A. T. Le, C. Jin, and H. Wei, *Attosecond and Strong-Field Physics Principles and Applications* (Cambrige University press, Cambridge, England, 2018).

[3] M. Drescher, M. Hentschel, R. Kienberger, M. Uiberacker, V. Yakovlev, A. Scrinzi, Th. Westerwalbesloh, U. Kleineberg, U. Heinzmann, and F. Krausz, Time-resolved atomic inner-shell spectroscopy, Nature (London) **419**, 803 (2002).

[4] A. Schiffrin, T. Paasch-Colberg, N. Karpowicz, V. Apalkov, D. Gerster, S. Muhlbrandt, M. Korbman, J. Reichert, M. Schultze, S. Holzner, J. V. Barth, R. Kienberger, R. Ernstorfer, V. S. Yakovlev, M. I. Stockman, and F. Krausz, Optical-field-induced current in dielectrics, Nature (London) **493**, 70 (2013).

[5] P. Colosimo, G. Doumy, C. I. Blaga, J. Wheeler, C. Hauri, F. Catoire, J. Tate, R. Chirla, A. M. March, G. G. Paulus, H. G. Muller, P. Agostini, and L. F. Dimauro, Scaling strong-field interactions towards the classical limit, Nat. Phys. **4**, 386 (2008).

[6] C. Vozzi, F. Calegari, E. Benedetti, S. Gasilov, G. Sansone, G. Cerullo, M. Nisoli, S. De Silvestri, and S. Stagira, Millijoule-level phase-stabilized few-optical-cycle infrared parametric source, Opt. Lett. **32**, 2957 (2007).

[7] T. Popmintchev *et al.* , Bright coherent ultrahigh harmonics in the keV X-ray regime from mid-infrared femtosecond lasers, Science **336**, 1287 (2012).

[8] E. J. Takahashi, T. Kanai, K. L. Ishikawa, Y. Nabekawa, and K. Midorikawa, Coherent Water Window X-Ray Generation by Phase-Matched High-Order Harmonic Generation in Neutral Media, Phys. Rev. Lett. **101**, 253901 (2008).

[9] N. Ishii, K. Kaneshima, K. Kitano, T. Kanai, S. Watanabe, and J. Itatani, Carrier-envelope phase-dependent high harmonic generation in the water window using few-cycle infrared pulses, Nat. Commun. **5**, 3331 (2014).

[10] S. L. Cousin, F. Silva, S. Teichmann, M. Hemmer, B. Buades, and J. Biegert, High-flux table-top soft X-ray source driven by sub-2-cycle, CEP stable, 1.85-μm 1-kHz pulses for carbon K-edge spectroscopy, Opt. Lett. **39**, 5383 (2014).

[11] B. E. Schmidt, P. Béjot, M. Giguere, A. D. Shiner, C. Trallero-Herrero, E. Bisson, J. Kasparian, J.-P. Wolf, D. M. Villeneuve, J. C. Kieffer, P. B. Corkum, and F. Légaré, Compression of 1.8 μm laser pulses to sub-two optical cycles with bulk material, Appl. Phys. Lett. **96**, 121109 (2010).

[12] G. J. Stein, P. D. Keathley, P. Krogen, H. Liang, J. P. Siqueira, C. L. Chang, C. J. Lai, K. H. Hong, G. M. Laurent, and F. X. Kärtner, Water-window soft X-ray high-harmonic generation up to the nitrogen K-edge driven by a kHz, 2.1μm OPCPA source, J. Phys. B: At. Mol. Opt. Phys. **49**, 155601 (2016).

[13] F. Silva, S. M. Teichmann, S. L. Cousin, M. Hemmer, and J. Biegert, Spatiotemporal isolation of attosecond soft X-ray pulses in the water window, Nat. Commun. **6**, 6611 (2015).

[14] G. J. Stein, P. D. Keathley, P. Krogen, H. Liang, J. P. Siqueira, C. L. Chang, C. Lai, K. H. Hong, G. M. Laurent, and F. X. Kärtner, Water-window soft x-ray high-harmonic generation up to nitrogen K-edge driven by a kHz, 2.1 μm OPCPA source, J. Phys. B: At. Mol. Opt. Phys. **49**, 155601 (2016).

[15] S. M. Teichmann, F. Silva, S. L. Cousin, M. Hemmer, and J. Biegert, 0.5-keV soft X-ray attosecond continua, Nat. Commun. **7**, 11493 (2015).

[16] J. Li, X. Ren, Y. Yin, Y. Cheng, E. Cunningham, Y. Wu, and Z. Chang, Polarization gating of high harmonic generation in the water window, Appl. Phys. Lett. **108**, 231102 (2016).

[17] J. Li, X. Ren, Y. Yin, K. Zhao, A. Chew, Y. Cheng, E. Cunningham, Y. Wang, S. Hu, Y. Wu, M. Chini, and Z. Chang, 53-Attosecond X-ray pulses reach the carbon K-edge, Nat. Commun. **8**, 186 (2017).

[18] T. Gaumnitz, A. Jain, Y. Pertot, M. Huppert, I. Jordan, F. Ardana-Lamas, and H. J. Wörner, Streaking of 43-attosecond soft-X-ray pulses generated by a passively CEP-stable mid-infrared driver, Opt. Exp. **25**, 27506 (2017).

[19] S. L. Cousin, N. Di Palo, B. Buades, S. M. Teichmann, M. Reduzzi, M. Devetta, A. Kheifets, G. Sansone, and J. Biegert, Attosecond Streaking in the Water Window: A New Regime of Attosecond Pulse Characterization, Phys. Rev. X **7**, 041030 (2017).

[20] Y. Mairesse and F. Quéré, Frequency-resolved optical gating for complete reconstruction of attosecond bursts, Phys. Rev. A **71**, 011401 (2005).

[21] J. Gagnon, E. Goulielmakis, and V. S. Yakovlev, The accurate FROG characterization of attosecond pulses from streaking measurements, Appl. Phys. B **92**, 25 (2008).

[22] K. Zhao, Q. Zhang, M. Chini, Y. Wu, X. Wang, and Z. Chang, Tailoring a 67 attosecond pulse through advantageous phase-mismatch, Opt. Lett. **37**, 3891 (2012).

[23] M. Chini, S. Gilbertson, S. D. Khan, and Z. Chang, Characterizing ultrabroadband attosecond lasers, Opt. Express **18**, 13006 (2010).

[24] P. D. Keathley, S. Bhardwaj, J. Moses, G. Laurent, and F. X. Kärtner, Volkov transform generalized projection algorithm for attosecond pulse characterization, New J. Phys. **18**, 073009 (2016).

[25] X. Zhao, H. Wei, Y. Wu, and C. D. Lin, Phase-retrieval algorithm for the characterization of broadband single attosecond pulses, Phys. Rev. A **95**, 043407 (2017).

[26] W. Yu, X. Zhao, H. Wei, S. J. Wang, and C. D. Lin, Method for spectral phase retrieval of single attosecond pulses utilizing the autocorrelation of photoelectron streaking spectra, Phys. Rev. A **99**, 033403 (2019).